International Journal of Nanoscience
Vol. 16, No. 4 (2017) 1760032 (9 pages)
#c World Scienti¯c Publishing Company
DOI: 10.1142/S0219581X17600328

Opto-Electronic Properties of Green Synthesized ZnS Nanostructures

Sujata Deb
Department of Electronics & Communication Technology
Gauhati University, Guwahati 781014, Assam, India
sujatabmk@gmail.com

P. K. Kalita
Department of Physics, Rajiv Gandhi University
Rono Hills Doimukh 791112, Arunachal Pradesh, India
pkkalitagc@gmail.com

P. Datta
Department of Electronics & Communication Technology
Gauhati University, Guwahati 781014, Assam, India
pranayee.datta@gmail.com

Received 10 March 2017
Accepted 10 May 2017
Published 25 September 2017

ZnS nanostructures are synthesized by a wet chemical route using starch as green capping agent under nitrogen environment. The as-prepared nanostructures are characterized structurally, optically and electrically. X-ray di®raction (XRD) spectra con¯rm that the zinc sul¯de (ZnS) nanoparticles have cubic phase (zinc blende). UV–Vis spectrum of the sample clearly shows that the absorption peak exhibits blue shift compared to their bulk counterpart, which con¯rms the quantum con¯nement e®ect of the nanostructures. Its photoluminescence (PL) spectrum shows near band gap emission at 392 nm and extrinsic emission at 467 nm. The particle sizes calculated from XRD and UV studies are in fair agreement with high resolution transmission electron microscopy (HRTEM) results. Starch is found to be a noble capping agent in bringing quantum con¯nement. The synthesis under nitrogen environment has been observed to produce quality products by reducing the oxide traces. Moreover, the I–V characteristics under dark and illumination show that ZnS can be more suitable as photodetector.

Keywords: Green synthesis; nitrogen; photodetector.

1. Introduction

Existing era has witnessed a prompt advancement among various II–VI classes of inorganic semiconductor nanomaterials that have emerged as basic materials for applications in optoelectronics devices. Zinc Sul¯de (ZnS) belonging to II–VI class is a direct transition semiconductor with a larger band gap 3.72 eV (bulk material) at room temperature and has large exciton binding energy (□40 meV).[1,2] Therefore, it has been considered more suitable for visible-ultraviolet (UV)-light-based devices such as sensors/ photo detectors. ZnS

is also abundant, chemically stable and environmentally benign and thus extensively studied. However, the optoelectronic properties ZnS nanostructures have not been investigated in much detail relative to other II–VI class nanostructures. The various techniques approaches that have already been adopted for the synthesis of ZnS nanomaterials include aqueous precipitation routes, electro deposition, high temperature hot injection method, molecular beam epitaxy (MBE) and physical vapor deposition.[3] But, almost all of these techniques require highly sophisticated equipments and the use of toxic materials which are not environmentally gentle. Apart from the toxicity, these methods are also not cost effective, which is a major disadvantage for synthesis of nanoparticles at the industrial scale. Due to these difficulties, various eco-friendly and simple approaches for the synthesis of ZnS nanoparticles are being adopted. One such simple and environment friendly approach is the wet chemical approach using green capping agents. It has been perceived that a considerable number of surface atoms create high surface energy nanoparticles, making them very reactive. Thus, systems without protection of their surfaces can have aggregation. From this perspective, capping agents play a great role. Usage of starch as a "green" passivator has recently become an active research area for being ecologically friendly and non-toxic. Several authors[4] have stated the use of starch to synthesis nanostructures. Starch is considered as a good bio-polymer as it has the polar groups in its structures, such as –OH.[5] The hydroxyl groups of polysaccharides also work to obtain uniform structures in addition to protect from aggregation.

In this paper, the microstructural, optical and electrical properties of starch capped ZnS nanostructures prepared via wet chemical technique under nitrogen environment are reported along with the fabrication of a heterostructure device (Schottky diode) with the configuration Al/(starch capped ZnS)/ITO. Emphasis is given on the estimation of the key diode parameters like the saturation current (I_s), barrier height (Φ_b), ideality factor (η), responsivity (R_λ) and quantum efficiency (η) under forward low bias region of the I–V curve.

2. Experimental

2.1. Synthesis

Analytical grade (Merck) chemical reagents are used in the synthesis as received without any alteration. For the synthesis of ZnS two approaches are considered. In the first approach (S1), under normal oxidation in air, ammonia solution (NH_4OH) as a complexing agent is introduced slowly under continuous stirring to 3% starch capped zinc acetate dihydrate [$Zn(CH_3COO)_2.2H_2O$] (0.5 M) ion solution, until the solution becomes clear and homogeneous for preparation at alkaline medium adjusting pH to 10 and then to this zinc complex ion (Zn^{2+}) solution (approx. 50 mL), 0.5 M thiourea ($NH_2CS.NH_2$) solution (approx. 100 mL) is added drop-wise under continuous stirring on a magnetic stirrer for about 2 h heating at 80°C for formation of ZnS. In the second approach (S2), under nitrogen environment, likewise, ammonia solution (NH_4OH) is added to 3% starch capped zinc acetate dihydrate [$Zn(CH_3COO)_2.2H_2O$] (0.5 M) ion solution. Later to this zinc complex ion (Zn^{2+}) solution (approx. 50 mL), 0.5 M thiourea ($NH_2CS.NH_2$) solution (approx. 100 mL) is added dropwise under constant stirring as in the first approach, on a magnetic stirrer for 2 h at 80°C for the formation of ZnS nanoparticles. The synthesized ZnS is then grown on cleaned ordinary glass slides as thin films and are stored in air tight desiccators at room temperature for characteristic analysis. Colloidal solutions are also taken for optical as well as morphological studies.

2.2. Development of Schottky diode

For the development of Schottky diode, required layer of as-prepared starch capped ZnS film is spin coated over 500 nm thick indium tin oxide (ITO) coated glass substrate using appropriate shaped masking arrangement. The starch capped ZnS film/ITO configuration is then placed in a thermal evaporation chamber where aluminium (Al) with 99.995% purity foils under high vacuum of 2×10^{-5} Torr are evaporated over the starch capped ZnS film/ITO structure to cast as the top counter electrode layer via suitable masking system. Thus, the final Schottky hetero-structure has the configuration as Al/(starch capped ZnS)/ITO, the active area of the device being 0.21 cm^2. For the photoconductivity study, the light is made incident on the glass part of the ITO-coated glass. The measurement of the sample is carried in the atmosphere without incorporation of any anti-reflectors. The experimental arrangement is then housed to study the device characteristics.

2.3. Characterization

The phase purity and crystalline size of the as-prepared products are characterized by X-ray diffractometer (Seifert 3003-TT) over an angular range of $20° < 2\theta < 70°$ in continuous scan mode with step scan 0.05 using Cu–K_α radiation ($\lambda = 1.5406$ Å). Structural morphologies are recorded on a high resolution transmission electron microscope (JEOL JEM-2100) operated at voltage 200 KV. Selected area electron diffraction (SAED) patterns are also taken along with prominently observed d-values in HRTEM measurements. Photoluminescence (PL) spectrum of the ZnO nanoparticles is recorded using a Hitachi FL spectrophotometer (model-F-2500), with excitation wavelength of 240 nm. Optical absorption spectrum is recorded using a Shimadzu UV–Visible spectrophotometer (model-UV-1800), in the range of 200 to 800 nm. FTIR spectrum of the as-prepared sample is recorded with FTIR spectrometer (IR affinity-1, Shimadzu, Japan) temperature 25°C with 30 number of scans in the wave number range of 4000–400 cm^{-1}. Keithley 2612A System Source Meter is employed for precision current–voltage measurements of the as-fabricated devices.

3. Results and Discussion

3.1. Structural and morphological analysis

The XRD patterns of as-prepared 3% starch capped 0.5 M ZnS nanostructures prepared in air and under nitrogen flow are shown in Fig. 1. The samples show main diffraction peaks corresponding to cubic phase structure. Sample ZnS (S1) under air environment shows prominent diffraction peaks at 28.60° (111), 32.85° (200), 47.7° (220), 56.0° (311) and 59.02° (222) whereas the sample ZnS (S2) under nitrogen environment shows peaks at 28.25° (111), 47.94° (220) and 56.67° (311) corresponding to the cubic zinc blende.[6]

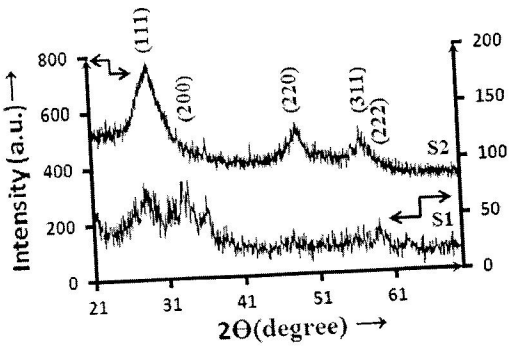

Fig. 1. XRD spectra of starch capped ZnS samples.

The diffraction peaks show a face centred cubic zinc blende structure with lattice constants, $a = 5.40$ Å (S1) and 5.46 Å (S2) that are in good agreement with standard JCPDS data (JCPDS file 05-0566). XRD pattern of S1 clearly specifies the presence of hydroxide traces along with the principal phase of ZnS. The occurrence of the oxide peak may be due to air which generally occurs in an open environment. Oxygen from air may diffuse through empty space in the sample and oxidize during the film formation. The abundance of oxide phases may affect the product in terms of crystallinity and purity. However, in sample S2, it has been observed that the number of oxygen peaks has greatly reduced, being prepared under nitrogen environment. Moreover, it shows broad diffraction peaks indicating the formation of mono-dispersed nanosize ZnS particles. Hence, it can be inferred that the nitrogen environment supports the strong confinement along with high purity of the material. The average particle size, D, has been estimated by using Debye–Scherrer formula,[7]

$$D = \frac{0.9\lambda}{\beta \cos\theta}; \quad (1)$$

where λ is wave length of X-Ray (0.1541 nm), β is FWHM (full width at half maximum) of the most preferential peak and θ is diffraction angle.

The d-spacing of nanostructure is calculated by using Bragg's law as given below:

$$2d_{hkl} \sin\theta = \lambda; \quad (2)$$

where d = inter-planar separation and (hkl) refers to the Miller indices of the reflecting plane.

The lattice parameter, a, for a cubic system for each plane [h, k, l] is estimated by the following relation:

$$d_{hkl} = \frac{a}{\sqrt{h^2 + k^2 + l^2}} \quad (3)$$

The dislocation density, δ is defined as the length of dislocation lines per unit volume. It signifies the amount of flawlessness in the crystal and is estimated from the following equation:

$$\delta = \frac{1}{D^2}; \quad (4)$$

Table 1. Structural parameters of ZnS sample (S2).

Sample Code	Observed Value of 2□(Degree)	Lattice Plane (h k l)	Spacing d(Å)	Lattice Parameter a(Å)	Av. Particle Size D (nm)	Av. Dislocation Density □□ $10^{□3}$(nm)$^{□2}$	Av. Strain " □ $10^{□3}$
S□	28.25	ZnS (111)	3.1593	a ¼ 5:46	6.95	25	5.54
	47.94	ZnS (220)	1.8978				
	56.67	ZnS (311)	1.6244				

Strain, ", of the composite thin □lm is determined from the following formula:

$$" ¼ \frac{□\cos□}{4}; \quad (5)$$

where □ is the FWHM and □ is the di®raction angle.

The calculated particle size for S2 is 6.95 nm which is in fair agreement with size estimated from HRTEM studies. The microstructural parameters of the as-prepared sample, S2, are summarized in Table 1.

The HRTEM image (S2) exhibits a good distribution of spherical ZnS nanoparticles (Fig. 2). The corresponding ring-like SAED pattern can be indexed to (111), (220) and (311) crystal planes of cubic structure that ascertain the polycrystalline nature of ZnS. The images clearly show the d-value of 0.27 nm corresponding to (200) of cubic ZnS. The average particle size of the nanostructures is in the range of 4.35–5.5 nm (S2). Thus, the particle size from HRTEM analysis is in reasonable agreement with size from XRD analysis.

3.2. Optical study

The UV–Vis absorption spectrum of the as-prepared sample, ZnS (S2) is shown in Fig. 3. Absorption edge is located approximately at around 310 nm. The energy band gap of material is calculated using Tauc's relation[8] and the calculated band gap value for S2 is 4.0 eV, which is blue shifted from that of its bulk counter-part (3.72 eV) due to the e®ect of quantum con□nement. Using the obtained band gap, the average size of the articles is obtained from the Brus equation,[9] as given below:

$$(E_g □ E_a)^{□1=2} ¼ □D; \quad (6)$$

where

□ ¼ 0:49 nm$^{□1}$eV$^{\frac{1}{2}}$,
E_g ¼ band gap of the nanomaterial,
E_a ¼ bulk band gap and
D ¼ the nanoparticle size.

The average size of the particles as obtained from the Brus equation is 3.86 nm (S2). Predominantly, the OH ligand of starch is very much e®ective in bringing the quantum con□nement in ZnS nanostructures.

Figure 4 shows the room temperature PI spectrum of ZnS (sample, S2) measured at 240 excitation wavelength with near band gap emission at 392 nm and another extrinsic emission at 467 nm.

The observed near band gap PL is a consequence of radiative recombination of electrons and holes

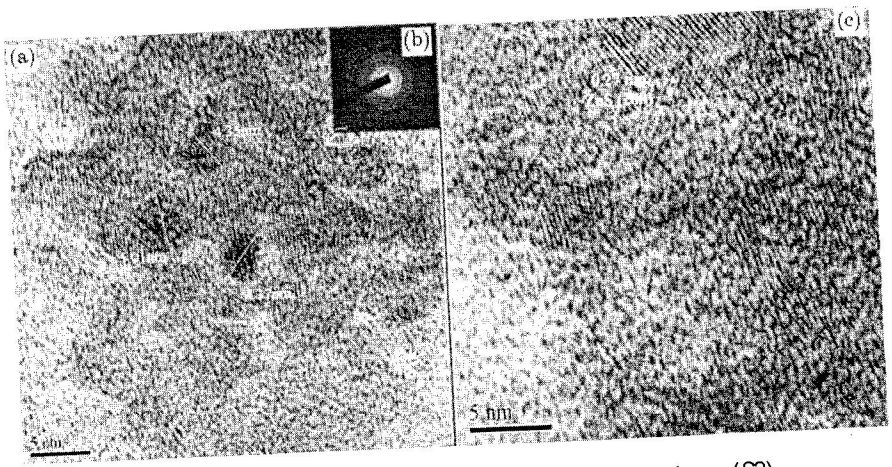

Fig. 2. HRTEM of 3% starch capped ZnS nanostructures (S2).

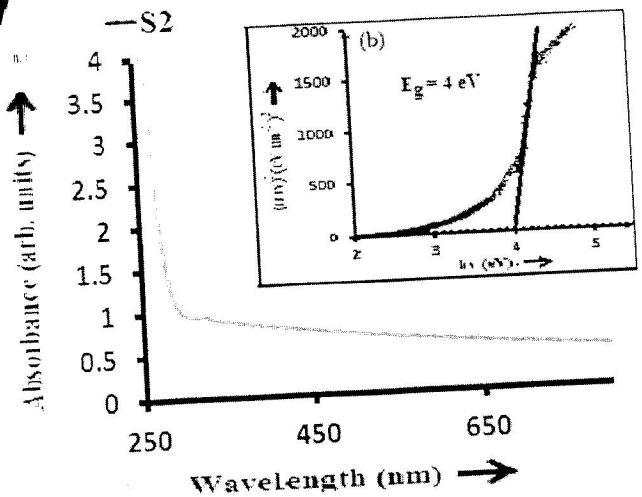

Fig. 3. UV absorption spectrum of ZnS under nitrogen (S2).

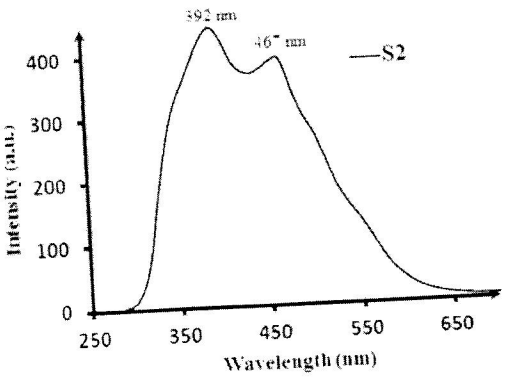

Fig. 4. PL emission spectrum of ZnS under nitrogen (S2).

con¯ned in nanoparticles, whereas extrinsic emission is ruled by various defects. Surface of a nanoparticle is very sensitive and reactive. There are lots of unsaturated bonds on the surface of ZnS forming gap surface states. More precisely, the blue emission at 467 nm may be attributed to the trapped luminescence that arises from the $Zn^{2þ}$ vacancies, $S^{2□}$ vacancies and surface states. In the case of ZnS, the calculated value of Stokes shift is 82. Its high value re°ects the existence of plenty of defect states in the synthesized ZnS nanostructures. The optical behavior of the sample, S2, is summarized in Table 2.

FTIR spectrum is used to calculate various functional groups present in the ZnS sample and are shown in Table 3. The FTIR spectrum of S2 is shown in Fig. 5.

In this study, an absorption band at 445 $cm^{□1}$ is attributed to the stretching vibrations band of ZnS,[9] indicating the presence of zinc sulphide nanoparticles. Furthermore, the observed characteristic peaks of ZnS at around 911 and 631 $cm^{□1}$ match well with the reported results of other workers.[10] The observed peaks at 1554 $cm^{□1}$–1608 $cm^{□1}$ represent the C¼O stretching modes and the broad absorption peaks in a range of 3162 $cm^{□1}$–3354 $cm^{□1}$ may be attributed to O–H stretching modes.[11] FTIR study has also become useful to identify the capping of the particles by starch. The very strong peak at 1146 $cm^{□1}$ may be contributed by □C–O groups of starch. The broad and strong peak at 3354 $cm^{□1}$ can be attributed to the □OH groups of starch. Thus, the IR study con¯rms the presence of □C–O and □OH groups of starch that facilitate easy binding with the metal surface.[12] So it can be concluded that ZnS nanoparticles are well capped and put in a nutshell by starch molecules.

3.3. Conductivity measurement

For the conductivity study, the I–V characteristic of the starch capped ZnS (S2) is studied using Cu as a contact electrode with gap type arrangement. The gap-type con¯guration is designed in a co-planar system with the as-prepared ¯lm deposited in the gap between two parallel Cu (electrode) coated stripes with spacing of 1.5 mm; the e®ective cross-sectional area being 5 mm □ 1.5 mm. The current °owing through the ¯lm is measured within the applied bias using a Keithley 2612A System source meter.

The current–voltage curve [Fig. 6(a)] of S2 in dark shows linear characteristics passing through the origin, which con¯rms the Ohmic nature of electrode-¯lm contact. Hence, the Ohmic behavior exhibits the inherent conductivity property of the ZnS ¯lms. The free charge carriers that remain

Table 2. Summarized optical behavior of as-synthesized ZnS nanostructure (S2).

	UV–vis		PL Emission Peak (nm)		
Sample Code	Absorption peak, □a (nm)	Band gap, E_g (eV)	Near Band Gap Emission, □e	Impurity Emission, □i	Stokes Shift (nm)
S2	310	4	392	467	82

Table 3. Various functional groups in 3% starch capped ZnS.

Vibrational Mode	Absorption (cm^{-1}) Region	Relative Intensity
Zn–S stretching	445, 911 and 631	Medium
C¼O stretching	1554–1608	Medium
O–H stretching	3162–3354	Strong and broad
C–O stretching	1146	Medium

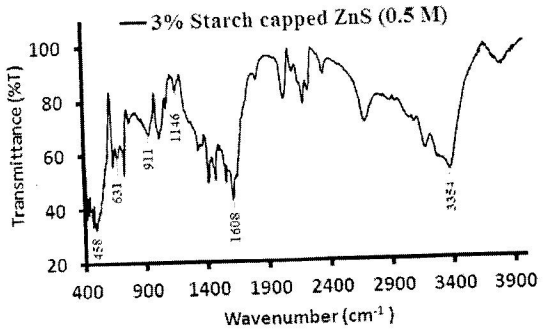

Fig. 5. FTIR of ZnS under nitrogen (S2).

available at room temperature may provide the current through the as-prepared ¯lms.

An Ohmic contact is said to be perfect when I–V characteristic is linear and the photovoltaic e®ect is not seen under illumination.[13] For this purpose, I–V curves of the sample with this same geometry are also studied under illumination (Blue LED of wavelength, ¼470 nm and power, P ¼ 8:5 mW) and are displayed in Fig. 6(b). The electrical performance of the samples did not show any photovoltaic e®ect but is found to be photosensitive. From the I–V characteristics, the resistivity and the conductivity of the ZnS ¯lm are calculated both in dark and under illumination and are shown in Table 4. The values of resistivity of ZnS decrease under illumination and hence conductivity increases.

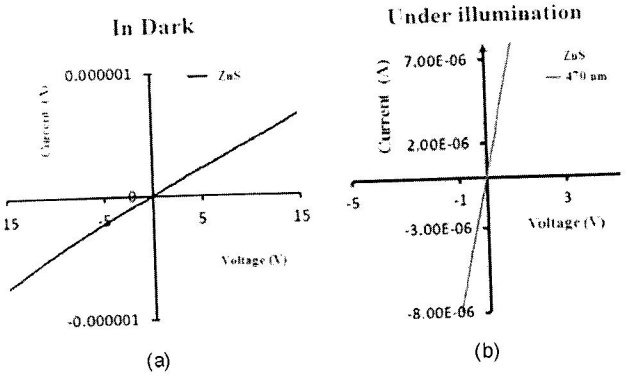

Fig. 6. I-V characteristics of as-prepared ZnS sample (S2) at room temperature 300 K.

The conductivity of ZnS nanocomposites under illumination is found to be more with a di®erence of two orders of magnitude than in dark.

3.4. Device (Schottky diode) performance parameters

Current–voltage measurement of Schottky diodes based on ZnS nanostructure (S2) has been recorded in the forward and reverse directions at room temperature. The performance of a practical Schottky diode in the present work is characterized by its dark current and photo-current (Figs. 7 and 8).

The I–V curve of as-fabricated sample has shown signi¯cant recti¯cation characteristics that may be originated due to the presence of an electrostatic barrier between the metal (electrode, Al) and the semiconductor (ZnS) as they have di®erent work functions. This Schottky barrier diode, being a sandwich system, has a surface contact rather than point contact, and this large contact area between aluminum and a semiconductor provides some advantages over point contact diode. Surface defects create band gap states in the semiconductor, leading to a distribution of electronic levels in the band gap at the interface and the Fermi level may get pinned and the Schottky barrier junction is thus formed.

From the dark characteristic, it is found that the reverse currents are very feeble and the forward currents increase severely with the applied bias voltage. The fundamental device parameters like the saturation current (I_s), barrier height (Φ_b) and ideality factor (η) of Schottky diodes based on ZnS are estimated using the forward low bias region of the I-V curve.

The Schottky barrier is normally estimated from I-V characteristics, supposing thermionic emission to be the dominant conduction mechanism. Thus, the I-V characteristics for the Schottky diode are analyzed using the following relations:

$$I = I_s \exp\left(\frac{qV}{\eta k_B T}\right)\left[1 - \exp\left(-\frac{qV}{k_B T}\right)\right], \qquad (7)$$

where I is diode current and the saturation current I_s is expressed as

$$I_s = SA^{*}T^{2}\exp\left(\frac{-q\Phi_b}{k_B T}\right), \qquad (8)$$

Table 4. Resistivity, □ and conductivity, □ of the as-prepared sample (S2) in dark environment and under illumination.

Material	Resistivity, □¼RA/L (□m)		Conductivity, □¼1=□ð□mÞ□1	
	DARK	Under Illumination BLUE LED 2.64 eV (P ¼8:5 mW, □¼470 nm)	DARK	Under Illumination BLUE LED 2.64 eV (P ¼8:5 mW, □¼470 nm)
ZnS	7.50Eþ08	4.46Eþ06	1.33E□09	2.24E□07

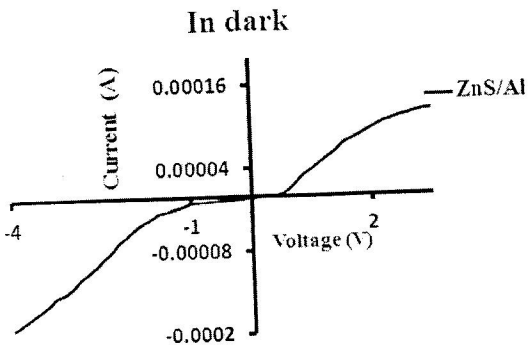

Fig. 7. I–V characteristics of as-prepared ZnS sample (S2) at room temperature 300 K.

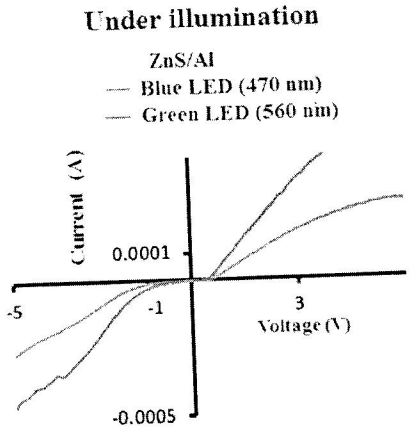

Fig. 8. I-V characteristics of as-prepared ZnS sample at room temperature 300 K.

Here, S is the cross-sectional diode area (metal/semiconductor interface)

V is bias across the interface.

T is the temperature in Kelvin, q is the electronic charge.

k_B is the Boltzmann constant (8:62 □ $10^{□5}$ eV$K^{□1}$); k_BT=q is the thermal voltage approximately 25.85 mV at 300 K.

□b is the e®ective Schottky barrier height.

A□ is the e®ective Richardson constant.

In the present work, the value of A* is calculated using the equation as

$$A^{□} ¼ 4□m_e □qk_B^2=h^3: \quad ð9Þ$$

n-type, $A^{□} ¼ 48 A/cm^2K^2$ with $m_e^{□} ¼ 0:40 m_o$; m_e^* being the electron e®ective mass.

□ is the ideality factor of the diode, which is a measure of how closely the diode follows the ideal diode equation.

The ideal diode equation typically assumes that all the recombination processes take place through band to band or recombination by means of traps in the majority regions from the device (explicitly, not in the junction) and the ideality factor, □, is equal to 1. However, recombination does take place by other means and in other regions of the device. These recombination paths produce ideality factors that deviate from the ideal value.

By the use of conventional method, the diode ideality factor is measured from the slope of linear region of the ln I-V plot. The slope gives q=□k_BT and thereby □ can be estimated whereas the saturation current (I_s) is extracted by extrapolating the linear part of ln I-V plot. Schottky barrier height □b controls the electronic transport across metal-semiconductor interface and its magnitude decides the e®ective operation of any semiconductor device. By substituting this I_s value in Eq. (10), the e®ective Schottky barrier height, □b is □nally determined.

$$□_b ¼ \frac{k_BT}{q} \ln \frac{□SA□T^2□}{I_s}: \quad ð10Þ$$

All the calculated Schottky diode parameters are represented in Table 5.

In the present work with Al as Schottky contact, the obtained value of Schottky barrier height at the Al/ZnS interface is 0.45 eV. Thus, a good rectifying contact has been established. A high value of Schottky barrier heights leads to low leakage currents. Further, the value of ideality factor for Schottky diode with ZnS is estimated as 1.52, which is close to an ideal diode behavior (n ¼ 1). The

Table 5. Key performance parameters of as-fabricated Schottky diode

Device type	Material	Saturation current, I_s (A)	Barrier height, ϕ_b (eV)	Ideality factor, η
Schottky diode	ZnS	3.00E-06	0.45	1.52

ideality factor close to 1 points toward the thermionic emission mechanism to be dominant.

The curves not only reveal rectifier characteristics but also a high response toward the light. As the light of particular power is incident to the sample film, it induces an increase in the photon-generated carriers that float toward the contact electrodes and a photocurrent is observed. Compared to the dark current value, the photocurrent value is much higher in the fabricated sample.

The performance of a practical photodiode is also characterized by its responsivity, R_λ at a particular wavelength. It is defined as the ratio of the generated photocurrent (I_P) to the incident radiation power (P) at a given wavelength.

$$\text{i.e.; } R_\lambda = \frac{I_P}{P}: \quad (11)$$

All the photons collected by a detector or a sensor are not converted to electron-hole pairs. The number of electrons created per incident photon that contribute to photocurrent is defined as the quantum efficiency, η and is stated as a percentage. It is correlated to responsivity by

$$\eta = R_\lambda(hc/q\lambda), \quad (12)$$

$$; \quad \eta = 1240\frac{R_\lambda}{\lambda}(\text{nm}), \quad (13)$$

where $h = 6.63 \times 10^{-34}$ J-s, is the Planck constant, $c = 3 \times 10^8$ m/s, is the speed of light, $q = 1.6 \times 10^{-19}$ C, is the electron charge, R_λ is the responsivity in A/W and λ is the wavelength in nm.[14]

The variation of responsivity, R_λ and quantum efficiency, η of the as-fabricated Schottky diode at 0.5 V bias condition are measured and are shown in Table 6.

Two different light sources are employed to determine responsivity and quantum efficiency of Schottky diode based on as-prepared nanostructures. Under blue and green illumination at 0.5 V, responsivity of ZnS is 2×10^{-4} A/W and 3.21×10^{-5} A/W, respectively. From the observed result, it can be understood that this device can be a promising candidate for visible detector application. However, the calculated values of responsivity under blue and green LED illumination are found to be low, which may mainly be due to absence of the direct band-to-band absorption in ZnS and weaker absorption at longer wavelengths. The earlier reported values of responsivity of many optical photodetectors in the UV and visible region are found to be low, and they are still being used for light detection.[14] Thus, there is stimulated research on wide direct band gap materials for possible fabrication of sensitive optoelectronic devices to UV and visible light. Hence, devices with many such materials have already become commercially available. Wide band gap semiconductor, ZnSe, GaN-based UV photodetectors are previously reported.[14] However, issues need to be considered such as the high contact resistance between nanostructure films and electrodes, surface recombination problems associated with the high surface area of the nanostructures, etc. Further efforts such as improvement in Ohmic contact, structural optimization, and device integration, are necessary for this new technique to be competitive with the other systems. Hence, this can be a subject of further investigation.

Table 6. Responsivity, R_λ and quantum efficiency, η of the preferred as-fabricated Schottky photodiodes at a fixed 0.5 V bias voltage.

	Device Type: Schottky diode	
	Responsivity, R_λ (A/W)	Quantum Efficiency %
BLUE LED 2.64 eV ($P = 8.5$ mW, $\lambda = 470$ nm)	2.00E-04	0.05
GREEN LED 2.30 eV ($P = 6.2$ mW, $\lambda = 540$ nm)	3.21E-05	0.01

4. Conclusion

Green capped ZnS nanostructures have been successfully synthesized via chemical route. ZnS exhibits the polycrystalline nature having intense diffraction peaks along (111), (220) and (311) directions mainly due to cubic zinc blend phase in the present growth conditions. Nitrogen environment has been realized to eliminate the oxide traces

bring purity in the product. HRTEM images exhibit a spherical-shaped particle distribution for ZnS nanostructures. The size of the particles is quite in agreement with that of the measurement from XRD. The SAED pattern also confirms the polycrystalline nature of the sample. UV–Vis measurement studies of the samples clearly show that the ZnS quantum dots exhibit strong quantum confinement effect. PI spectrum of ZnS shows near band gap emission at 392 nm and extrinsic emission at 467 nm from inherent defects produced in the sample. I-V curves of ZnS sample in dark and illumination at room temperature show a linear nature without any rectification which demonstrates the Ohmic electrode (Cu)-film contact, thus revealing the conductivity nature of the films. Moreover, the I-V curve of the sample under illumination did not show any photovoltaic effect but is found to be photosensitive. The I-V characteristics of the as-fabricated heterostructure device with configuration Al/starch capped ZnS/ITO (Schottky diode) show rectifying nature indicating the formation of a Schottky contact between Al and Zinc chalcogenides. The fundamental diode parameters are estimated from the I-V measurements based on the ideal thermionic emission theory. Hence, considering the simple fabrication process and minimal cost, this kind of nanostructure is expected to be a suitable candidate for visible detector applications and can be a subject of further investigation.

Acknowledgments

Authors gratefully acknowledge the technical support of the Department of Chemistry, Gauhati University for UV–Visible and PL measurements, SAIF-GU and Centre for Nanotechnology, IIT-Guwahati for XRD analysis, Department of Physics, IIT-G for I-V characteristics and also the Sophisticated Analytic Instrument Facility (North Eastern Hill University) Shillong for HRTEM studies.

References

1. X. Huang, M. Willinger, H. Fan, Z. Xie, L. Wang, A. Hoffmann, F. Girgsdies, C. Leec and X. Meng, Nanoscale 6, 8787 (2014).
2. Q. Xiong, G. Chen, J. D. Acord, X. Liu, J. J. Zengel, H. R. Gutierrez, J. M. Redwing, L. C. Lew Yan Voon, B. Lassen and P. C. Eklund, Nano Lett. 4, 1663 (2004).
3. K. Mahmood, M. Asghar, N. Amin and A. Ali, J. Semicond. 36, 33001 (2015).
4. J. Soni and A. A. Koser, Open Int. J. Technol. Innov. Res. 16, 1 (2015).
5. A. Kołodziejczak-radzimska and T. Jesionowski, Materials (Basel). 7, 2833 (2014).
6. T. T. Nguyen, X. A. Trinh, L. H. Nguyen and T. H. Pham, Adv. Nat. Sci. Nanosci. Nanotechnol. 2, 35008 (2011).
7. V. D. Mote, Y. Purushotham and B. N. Dole, J. Theor. Appl. Phys. 6, 6 (2012).
8. A. Rahdar, World Appl. Program. 3, 56 (2013).
9. N. Qutub, Synthesis and Characterization of Nanomaterials, (Aligarh Muslim University, 2013, Thesis).
10. M. M. Duvenhage, NSTI-Nanotech 1, 543 (2010).
11. J. Coates, Encyclopedia of Analytical Chemistry (John Wiley & Sons Ltd., 2000).
12. U. S. Senapati, D. K. Jha and D. Sarkar, Res. J. Phys. Sci. Res. J. Phys. Sci. 1, 2320 (2013).
13. R. W. Smith, Phys. Rev. 97, 1525 (1955).
14. N. N. Jandow, H. Abu Hassan, F. K. Yam and K. Ibrahim, Photodetectors 3 (2009).